

Quantum Coherence in Photo-Ionization with Tailored XUV Pulses

Stefanos Carlström^{1,*}, Johan Mauritsson¹, Kenneth J. Schafer², Anne L’Huillier¹,
and Mathieu Gisselbrecht^{1,†}

¹*Department of Physics, Lund University, Box 118, 221 10 Lund, Sweden*

²*Department of Physics and Astronomy, Louisiana State University, Baton Rouge, LA 70803*

**Email: stefanos.carlstrom@gmail.com*

†Email: mathieu.gisselbrecht@sljus.lu.se

January 16, 2022

Abstract

Ionization with ultrashort pulses in the extreme ultraviolet (XUV) regime can be used to prepare an ion in a superposition of spin-orbit substates. In this work, we study the coherence properties of such a superposition, created by ionizing xenon atoms using two phase-locked XUV pulses at different frequencies. In general, if the duration of the driving pulse exceeds the quantum beat period, dephasing will occur. If however, the frequency difference of the two pulses matches the spin-orbit splitting, the coherence can be efficiently increased and dephasing does not occur.

1 INTRODUCTION

The wave nature of matter is central to the quantum mechanical description of the microcosmos; therefore coherence — a measure of the ability to produce stationary interference patterns — is an important property of any quantum system. An example of a coherent system is the superposition of two pure states, $|\psi\rangle = a|1\rangle + b|2\rangle$; such superpositions form the basis for the field of quantum

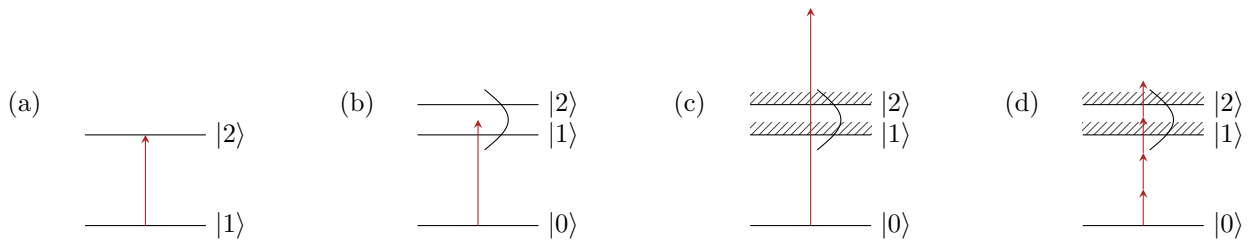


Figure 1: Different ways of preparing coherent superpositions using light; (a) excitation of a two-level system, such as those used for qubits in quantum information; (b) coherent excitation from the ground state to two excited bound states; (c) single-photon ionization, with the ion left in a superposition of substates; (d) strong-field ionization, also leaving the ion in a superposition of substates.

Element	Z	n	ΔE_{s-o} [eV]	T [fs]
Ne	10	2	0.09676024	42.8
Ar	18	3	0.17749368	23.3
Kr	36	4	0.665808	6.2
Xe	54	5	1.306423	3.2

Table 1: Some properties of heavy noble gases. ΔE_{s-o} is the spin-orbit splitting of the ionic ground state $n p^5 \ ^2P^o$. The quantum beat period, $T(= 2\pi\Delta E_{s-o}^{-1})$, is the intrinsic atomic clock associated to two states separated by an energy difference of ΔE_{s-o} .

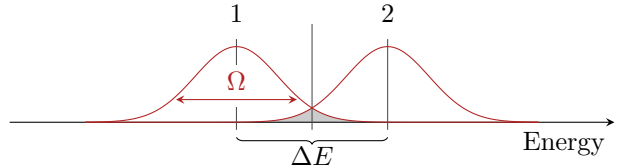


Figure 2: Overlap (shaded area) between two quantum paths (1 and 2) separated by ΔE . The spectral bandwidth, Ω , of the ionizing pulse is inversely proportional to the duration of the pulse; increasing the pulse duration thus leads to decreased overlap between the quantum paths.

information, where they are used to represent qubits. The manipulation of qubits for quantum computing necessarily requires that the coherence of the system is retained; if not, the information contained within the qubit is lost. In quantum optics, superpositions between two states may be created via a transition between the two states with an appropriately tailored pulse (e.g. a $\pi/2$ -pulse) [figure 1 (a)].

Superpositions of states can also be achieved by direct excitation using short light pulses [figure 1 (b)], provided the bandwidth of the pulse is larger than the energy difference (ω_{21}) between the two states. This requires a pulse duration short enough, $\tau \leq 2\pi/\omega_{21}$. If the superposition is successfully created, it may be observed through quantum beats (Teets et al. 1977; Salour and Cohen-Tannoudji 1977; Mauritsson et al. 2010; Tzallas et al. 2011) which usually last substantially longer than the pulse duration. The characteristic decay time is termed the *coherence time*. In the cases depicted in 1 (a) and (b), the light couples the bound states and enables coherent population transfer.

Another way to produce a superposition of states is via short-pulse ionization, when the ion is left in a coherent superposition of final states, e.g. due to spin-orbit interaction. This can be done using either high-frequency [figure 1 (c)] or high-intensity short-pulse [figure 1 (d)] radiation. As previously, the bandwidth of the ionizing pulse has to exceed the energy splitting between the ion states. Kurka et al. (2009) investigated case 1 (c) by photo-ionizing neon using short XUV pulses from a free-electron laser. A coherent superposition of the ionic fine-structure substates was prepared and probed by subsequent ionization. Using a strong laser field [figure 1 (d)], Goulielmakis et al. (2010) photo-ionized krypton, leaving the residual Kr^+ ion in a coherent superposition of the ionic substates. The quantum beat was observed by probing with a delayed attosecond (as) XUV pulse, as long as the duration of the ionizing pulse was shorter than the quantum beat period of the Kr^+ ion. This experimental activity stimulated an important theoretical effort to investigate the coherence of superpositions of states produced either directly by photo-excitation [figure 1 (b); Tzallas et al. 2011; Klünder et al. 2013], single-photon ionization [figure 1 (c); Nikolopoulos 2013], or strong-field ionization [figure 1 (d); Pabst et al. 2011, 2016].

As mentioned above, the creation of a coherent superposition in the cases depicted in figures 1 (b–d), requires sufficient bandwidth of the exciting/ionizing radiation. As the pulse duration increases, or the energy separation between electronic states increases, states become spectrally resolvable. Excitation/ionization to one state or the other can then be seen as distinguishable quantum paths taken by the system (see figure 2). When the spectral overlap between these quantum paths decreases, the coherence between states diminishes. While a spectral representation provides meaningful physical insight, it does not allow understanding how coherence is built-up in real time. Therefore, a temporal representation, based on an atomic clock constituted by the

quantum beat period, is very useful to determine whether decoherence will occur or not during light–matter interaction. As long as the pulse duration is shorter than a quantum beat period, the atomic clock will not dephase, since there is still appreciable overlap between the quantum paths (see figure 2). For ionization of noble gases, the available quantum beat periods span an order of magnitude (see table 1). However, ultrashort pulses are still necessary to manipulate the coherence.

In this article, we present a theoretical study of single-photon ionization of xenon atoms using XUV pulses, tailored in such a way that the quantum paths *always* overlap spectrally, providing a new ionization scheme to control and maximize the coherence between states, independent of the pulse duration. This is achieved by employing a bichromatic or multi-colour ionizing field, consisting of phase-locked harmonics such as those resulting from high-order harmonic generation (HHG), provided the spectral components fulfill a certain resonance condition. We investigate the tolerance of this resonance condition, i.e. how strict the requirements on the driving field are, with respect to the excitation frequencies, pulse duration, and temporal structure, for maintaining a certain level of coherence. We find the existence of resonant conditions, which correspond to a situation where multiple quantum paths lead to the same photo-electron state.

The paper is organized as follows; in the following section, we present our numerical calculations based on the fully correlated time-dependent Schrödinger equation (TDSE) in the case of weak-field ionization, as well as the theoretical tools that are used to calculate the evolution of the superposition of states in the presence of the driving field. We also introduce the density matrix formalism used to analyze the coherence of the quantum system. Atomic units are used throughout, unless otherwise stated. Using the numerical calculations, in section 3, we study ionization using two harmonic components, and investigate the relation between their energy separation and the spin–orbit splitting using a temporal model of the ionization dynamics. From this, we extract a generalized quantum beat condition. Finally in section 4, we derive a spectral model for the general case of ionization by multi-colour fields. This enables us to capture the essential physics of the observed phenomena. We conclude with a short discussion about the foundation of the work in relation to quantum mechanics, suggesting that coherence between states should exist as long as ionization pathways are indistinguishable by the measurement.

2 THEORETICAL FRAMEWORK

We are interested in studying the coherence of different ionic states produced by photo-ionization with tailored XUV pulses. To this end, we use as a model system noble gas ions, which have a spin–orbit splitting of the ground state ($np^5\ ^2P_{j_i}^o$, $j_i = 3/2, 1/2$), in particular xenon ($n = 5$).

Figure 3 shows a simplified diagram of photo-ionization of a np electron. The ionic ground state has a spin–orbit splitting, which in xenon is 1.3 eV. We ionize with a weak XUV pulse with two frequency components, whose difference is ω_0 . Absorption of the two frequency components, $\Omega_>$ and $\Omega_<$, leads to an ion in either $^2P_{3/2}^o$ or $^2P_{1/2}^o$, resulting in four different pathways. If the frequency difference is equal to the spin–orbit spacing, there will be two (indistinguishable) pathways to the same final photo-electron energy; we call this the *resonant case*. We introduce the *detuning ratio* $d \equiv \omega_0/\Delta E_{s-o}$, and study photoionization in the vicinity of this resonance ($d \approx 1$).

The calculations are performed by solving the time-dependent Schrödinger equation (TDSE) in a limited subspace,

$$i\partial_t|\Psi(t)\rangle = \mathcal{H}(t)|\Psi(t)\rangle, \quad (1)$$

#	Channel configuration
1	$np^5(^2P_{3/2}^o)kd\ ^2[1/2]_1$
2	$np^5(^2P_{3/2}^o)ks\ ^2[3/2]_1$
3	$np^5(^2P_{3/2}^o)kd\ ^2[3/2]_1$
4	$np^5(^2P_{1/2}^o)ks\ ^2[1/2]_1$
5	$np^5(^2P_{1/2}^o)kd\ ^2[3/2]_1$
6	$nsnp^6(^2S_{1/2})kp\ ^2[1/2]_1$
7	$nsnp^6(^2S_{1/2})kp\ ^2[3/2]_1$

Table 2: Ionization channels accessible via one-photon ionization from the valence shell of a noble gas (final $J = 1$), in the case of jK coupling.

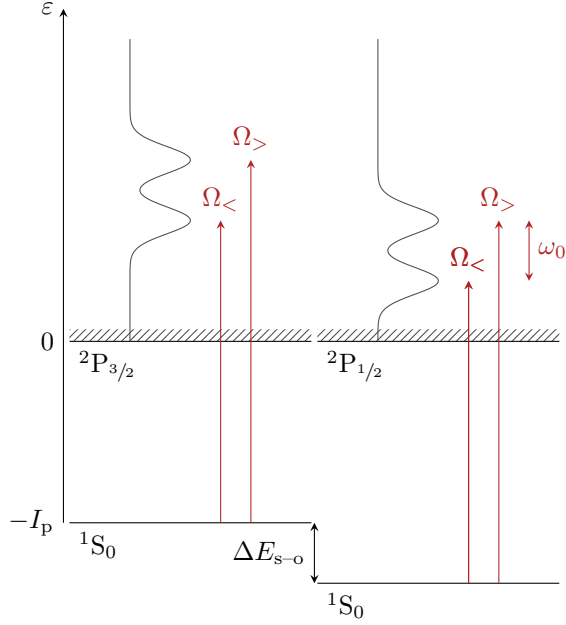


Figure 3: Schematic energy diagram of a noble gas (heavier than He, i.e. with a spin-orbit splitting of the first ionic ground state $np^5\ ^2P_{j_i}$, $j_i = 3/2, 1/2$) photo-ionized with a tailored XUV pulse consisting of two frequencies with $\Omega_> - \Omega_< = \omega_0$. The energy scale is that of the photo-electron kinetic energy, which depends on the final ion state, $^2P_{3/2}$ or $^2P_{1/2}$. It can be seen from the diagram that there are four pathways to the continuum. If $\omega_0 \approx \Delta E_{s-o}$, two of the quantum paths (absorption of $\Omega_<$ and the ion in $^2P_{3/2}$; absorption of $\Omega_>$ and the ion in $^2P_{1/2}$) lead to the same photo-electron energy.

where the Hamiltonian in the dipole approximation is

$$\mathcal{H}(t) = \mathcal{H}_0 + \mathcal{E}(t)z. \quad (2)$$

\mathcal{H}_0 is the atomic Hamiltonian, $\mathcal{E}(t)$ the electric field, and z is the dipole operator for linear polarization along the z axis. The solution is found by propagating the initial state (the neutral ground state) to time t

$$|\Psi(t)\rangle = \mathcal{U}(t, 0)|\Psi_0\rangle, \quad (3)$$

where the short-time propagator $\mathcal{U}(t + \Delta t, t)$ is approximated by a Magnus (1954) propagator of fourth order (Saad 1992; Alvermann et al. 2012).

The time-dependent wavefunction is expanded as

$$|\Psi(t)\rangle = c_0(t)|\Psi_0\rangle + \sum_i \sum_\ell \int d\varepsilon c_i^\ell(t; \varepsilon)|i\varepsilon\ell\rangle, \quad (4)$$

where $|\Psi_0\rangle$ is the ground state $ns^2np^6\ ^1S_0$ with energy $-I_p$, $c_0(t)$ the complex, time-dependent amplitude, i denotes the final state of the ion, and $\varepsilon\ell$ the quantum state of the photo-electron with angular momentum ℓ and energy ε (related to the momentum k by $\varepsilon = k^2/2$). The ionization channels formed by different possible combinations of i and ℓ , are listed in table 2, in the case of jK coupling. jK (or pair) coupling is defined as (Cowan 1981) $\mathbf{j}_i + \boldsymbol{\ell} = \mathbf{K}$ and $\mathbf{K} + \mathbf{s} = \mathbf{J}$, where \mathbf{j}_i is the total angular momentum of the parent ion, which couples to the angular momentum of the electron $\boldsymbol{\ell}$ to form an intermediate \mathbf{K} . The levels are then written as $\gamma_i(^{2S+1}L_{j_i})k\ell\ ^{2S+1}[K]_J$, where γ_i is the electron configuration of the ion.

The *Ansatz* (4) turns the TDSE (1) into a set of coupled ordinary differential equations (ODE):

$$i\partial_t \mathbf{c}(t) = \mathbf{H}(t)\mathbf{c}(t), \quad (1^*)$$

where the vector $\mathbf{c}(t)$ consists of the expansion coefficients in (4), and the *Hamiltonian matrix* is given by

$$\begin{aligned} \mathbf{H}(t) = & -|\Psi_0\rangle I_p \langle \Psi_0| + \sum_{i\ell} \int d\varepsilon |i\varepsilon\ell\rangle \varepsilon \langle i\varepsilon\ell| \\ & + \mathcal{E}(t) \left[\sum_{i\ell} \int d\varepsilon |i\varepsilon\ell\rangle \langle i\varepsilon\ell| z |\Psi_0\rangle \langle \Psi_0| + \sum_{i'\ell'} \int d\varepsilon' |i\varepsilon\ell\rangle \langle i\varepsilon\ell| z |i'\varepsilon'\ell'\rangle \langle i'\varepsilon'\ell'| + \text{c.c.} \right]. \end{aligned} \quad (2^*)$$

In the field-free basis, \mathbf{H}_0 is simply a diagonal matrix, with the energies of the photo-electron with respect to the lowest ionization threshold as matrix elements. The interaction term couples the ground state to the continua and the continua to each other. In the weak-field limit, however, the partial-wave expansion is restricted to total angular momentum $J \leq 1$, i.e. no multi-photon processes are considered. Furthermore, ionization is only allowed from the outer np shell (photo-electron energies in the range 0 eV to 11 eV in the case of xenon), to avoid autoionization of embedded Rydberg states in the vicinity of the $nsnp^6 \ ^2S_{1/2}$ threshold (that is, channels 6 and 7 in table 2 need not be considered). We also neglect mixing of singlet and triplet terms. Thus, the only non-zero matrix elements of the dipole operator z are $\langle i\varepsilon\ell|z|\Psi_0\rangle$ (and the complex conjugate). The basis functions ($|\Psi_0\rangle$ and $|i\varepsilon\ell\rangle$) and the dipole matrix elements ($\langle i\varepsilon\ell|z|\Psi_0\rangle$) are determined using ATSP2K (multi-configurational Hartree–Fock; Froese Fischer et al. 2007) and BSR (close-coupling R -matrix approach; Zatsarinny 2006; Zatsarinny and Froese Fischer 2009). The dipole matrix elements are spin-averaged by BSR.

The analysis of the coherence is made using the density matrix formalism [Landau and Lifshitz 1977, §14], where the full *density matrix* operator is formed from the wavefunction $|\Psi(t)\rangle$ obtained by solving (1) (time dependence t omitted below, for brevity)

$$\rho_T = |\Psi\rangle \langle \Psi|, \quad (5)$$

with matrix elements of the continuum block

$$\rho_{i_1 i_2}^{\ell_1 \ell_2}(\varepsilon_1, \varepsilon_2) \equiv c_{i_1}^{\ell_1}(\varepsilon_1) c_{i_2}^{\ell_2*}(\varepsilon_2). \quad (6)$$

We reduce this density matrix to an ion–channel density matrix by first taking the trace over the photo-electron energy ε :

$$\begin{aligned} \rho_{i_1 i_2}^{\ell_1 \ell_2} & \equiv \int d\varepsilon \langle \varepsilon | \Psi \rangle \langle \Psi | \varepsilon \rangle = \int d\varepsilon \sum_{i_1 i_2} \sum_{\ell_1 \ell_2} \int d\varepsilon_1 d\varepsilon_2 \langle \varepsilon | i_1 \varepsilon_1 \ell_1 \rangle c_{i_1}^{\ell_1}(\varepsilon_1) c_{i_2}^{\ell_2*}(\varepsilon_2) \langle i_2 \varepsilon_2 \ell_2 | \varepsilon \rangle \\ & = \sum_{i_1 i_2} \sum_{\ell_1 \ell_2} \int d\varepsilon |i_1 \ell_1\rangle \rho_{i_1 i_2}^{\ell_1 \ell_2}(\varepsilon, \varepsilon) \langle i_2 \ell_2|. \end{aligned} \quad (7)$$

Finally, we construct the ion density matrix by tracing over the photo-electron angular momenta:

$$\rho_{i_1 i_2} \equiv \sum_{\ell} \sum_{i_1 i_2} \sum_{\ell_1 \ell_2} \langle \ell | i_1 \ell_1 \rangle \rho_{i_1 i_2}^{\ell_1 \ell_2} \langle i_2 \ell_2 | \ell \rangle = \sum_{\ell} \sum_{i_1 i_2} |i_1\rangle \rho_{i_1 i_2}^{\ell \ell} \langle i_2|. \quad (8)$$

The diagonal elements (ρ_{mm}) of this matrix are the populations in each of the ionic states, while the off-diagonal elements (ρ_{mn}) contain the coherences between the ionic states. The only non-zero off-diagonal elements are those corresponding to channels for which all quantum numbers are the same (except for the angular momentum of the ion); i.e. only $\rho_{35} = \rho_{53}^* \neq 0$. Decoherence due to decay (through dipole-forbidden interaction) from the upper ionic state to the lower, is neglected.

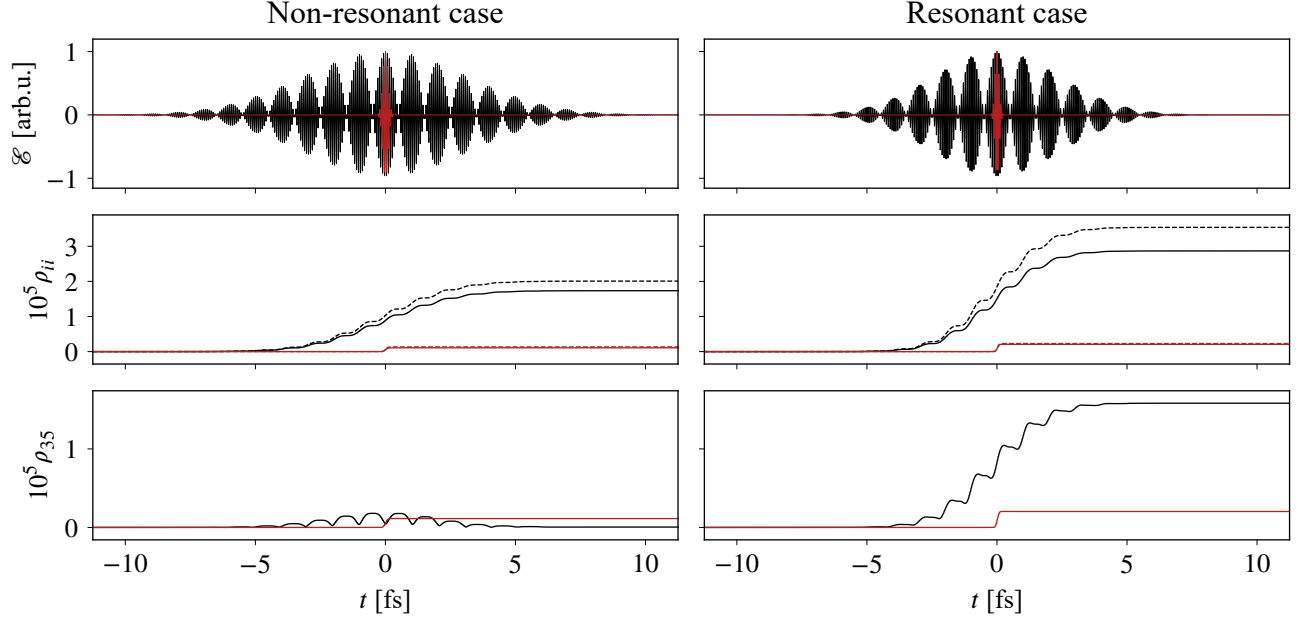


Figure 4: Real-time coherence build-up, for the case of ionization with two harmonics, 13 and 14 of a fundamental frequency $d\Delta E_{s-o}$, in the non-resonant case ($d = 1.3$) left and the resonant case ($d = 1$) right. The upper panels show the driving fields used; the red curve corresponds to a pulse duration (FWHM of the temporal intensity profile) of 500 as while the black curve corresponds to a pulse duration of 15 fs. The middle panels show the populations in the residual ionic substates (solid: contribution from channel 3 to ${}^2P_{3/2}^o$; dashed: contribution from channel 5 to ${}^2P_{1/2}^o$), which increase with time. The lower panels show the induced coherence between the ionic substates, which is built up over time. For the short-pulse case, there is always coherence left at the end of the pulse, while for the longer pulse duration, the resonance criterion has to be fulfilled $d \approx 1$ for this to happen. The lower population in the non-resonant case is explained by the decrease in photoionization cross-section with increasing photon energy.

3 THE BICHROMATIC CASE

We investigate the real-time build-up of coherence with a XUV pulse of short or long duration in the non-resonant case (figure 4, left) and the resonant case (figure 4, right). The electromagnetic fields are presented in the upper panels. In both cases, they consist of harmonics 13 & 14 of a fundamental driving field, and a peak intensity of 10^8 W cm^{-2} . The short-pulse duration is 500 as, while the long-pulse duration is 15 fs resulting in the formation of a periodic beating of the XUV pulse. Regardless of the pulse duration, the population in the ionic substates (middle shown in solid and dashed lines) increases as the pulse ionizes the atom. The population is proportional to the integral of the pulse intensity, hence the appearance of steps in the population.

3.1 The non-resonant case.

We first consider the non-resonant case (left panels of figure 4), where the fundamental driving frequency is $\omega_0 = 1.3\Delta E_{s-o}$. For a short pulse duration, the coherence increases during the interaction and stays constant after the pulse has passed. In contrast, for long pulse duration, the coherence first builds up, and then vanishes at the end of the pulse. The decoherence time, i.e. the time from the onset of the pulse to the decrease of the coherence (see lower panel of figure 4), is approximately equal to the quantum beat period $T = 2\pi/\Delta E_{s-o}$ of the ionic substates; for

xenon with a spin-orbit splitting of 1.3 eV, it is 3.2 fs. This is similar to what was observed by Goulielmakis et al. (2010), where the interference pattern, present in the transient absorption signal, disappeared when the ionizing infrared pulse exceeded the quantum beat period of 6.2 fs of krypton.

3.2 The resonant case. A generalized quantum beat condition.

In the resonant case (right panels of figure 4), the situation is completely different. The coherence is built up during all the interaction time, and remains after the end of the pulse. We can understand the existence of this resonance condition, using a simple two-excited-state model. The two excited states (labelled $|1\rangle$ and $|2\rangle$, for simplicity) correspond to the ionic substates, the populations of which result from a periodic sequence of ionization events (occurring at times t_k , $k \in \mathbb{N}$) from the ground state (labelled $|0\rangle$). We express this model using an inhomogeneous TDSE for the excited superposition $|\Psi(t)\rangle = c_1(t)|1\rangle + c_2(t)|2\rangle$, where the ground state constitutes a source term:

$$i\partial_t|\Psi(t)\rangle = \mathbf{H}_0|\Psi(t)\rangle + \mathcal{E}(t)(z_{10}|1\rangle + z_{20}|2\rangle), \quad \mathbf{H}_0 \equiv E_1|1\rangle\langle 1| + E_2|2\rangle\langle 2|, \quad z_{i0} \equiv \langle i|z|0\rangle. \quad (9)$$

Assuming no initial excited population, the solution of (9) is given by

$$|\Psi(t)\rangle = \exp(i\mathbf{H}_0 t) \left\{ \int^t dt' \mathcal{E}(t') [e^{-iE_1 t'} z_{10}|1\rangle + e^{-iE_2 t'} z_{20}|2\rangle] \right\} \quad (10)$$

If we assume that $\mathcal{E}(t)$ is a train of pulses, separated by $\Delta t \equiv t_k - t_{k-1}$, we can write the field as

$$\mathcal{E}(t) = \tilde{\mathcal{E}}(t) \left[\sum_k \delta(t_k) e^{i\phi_{XUV}(t_k)} \right],$$

where $\tilde{\mathcal{E}}(t)$ is a slowly varying envelope. The solution to the two-excited-state system in this case is

$$\begin{aligned} |\Psi(t)\rangle &= \exp(i\mathbf{H}_0 t) \sum_k \tilde{\mathcal{E}}(t_k) e^{i\phi_{XUV}(t_k)} [e^{-iE_1 t_k} z_{10}|1\rangle + e^{-iE_2 t_k} z_{20}|2\rangle] \\ &= \sum_k \tilde{\mathcal{E}}(t_k) e^{i\phi_{XUV}(t_k)} [e^{-iE_1(t_k-t)} z_{10}|1\rangle + e^{-iE_2(t_k-t)} z_{20}|2\rangle] \\ &= \sum_k \tilde{\mathcal{E}}(t_k) e^{i[\phi_{XUV}(t_k) - E_1(t_k-t)]} z_{10} [|1\rangle + \tilde{z} e^{-i\Delta E(t_k-t)} |2\rangle], \end{aligned} \quad (10^*)$$

where $\tilde{z} \equiv \langle 2|z|0\rangle / \langle 1|z|0\rangle$ is the relative dipole matrix element independent of the instant of ionization, and — assuming ionization solely into an unstructured continuum — independent of final electron energy and $\Delta E \equiv E_2 - E_1$, as well.

For the two substates to remain coherent, we require that no dephasing is introduced by pulses in the train. Since subsequent pulses are separated in time by Δt , this is equivalent to requiring that the phase argument in (10*) fulfills $\Delta E(t_k - t_a) = \Delta E \Delta t (k - a) = 2\pi$, $k, a \in \mathbb{N}$, or

$$\Delta t = \frac{2\pi r}{\Delta E} = rT, \quad (11)$$

is fulfilled, for any integer r . Δt is a multiple of the quantum beat period for an energy separation ΔE , which does not depend on the duration of the XUV pulse. In the spectral domain, this corresponds to requiring the final electron kinetic energy to be the same.

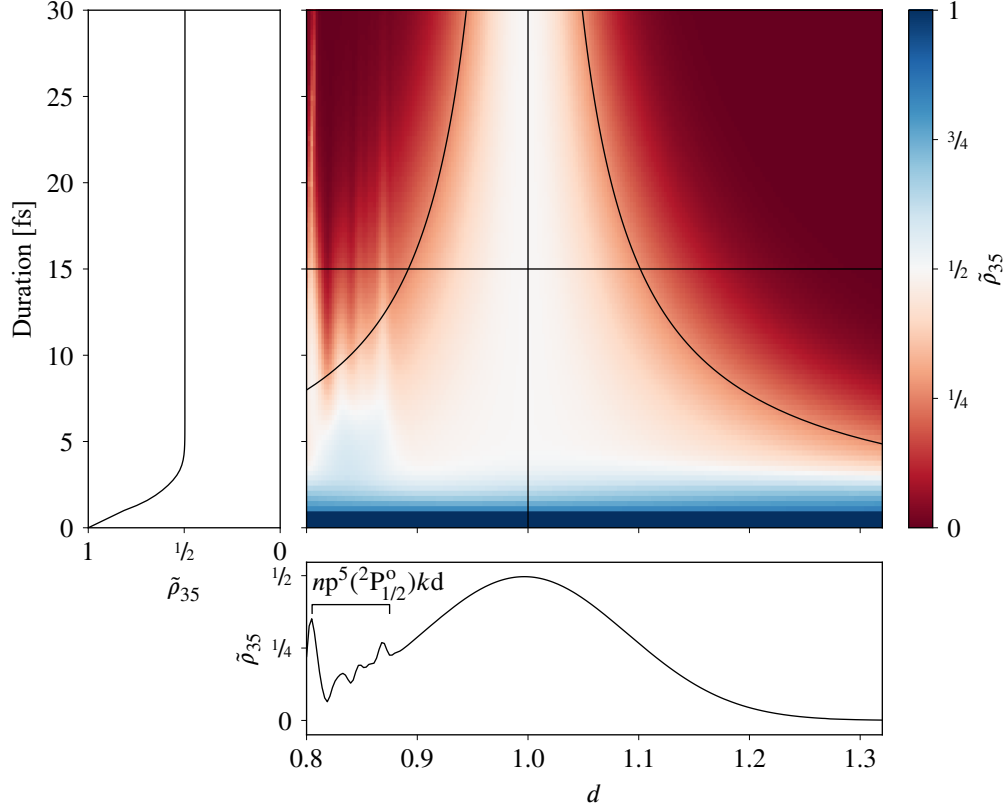


Figure 5: Degree of coherence as a function of pulse duration (FWHM of temporal intensity profile) and detuning ratio d . The hyperbolas in the main panel indicate the ‘coherence bandwidth’ within which $\tilde{\rho}_{35} > (2\sqrt{e})^{-1}$. The black horizontal/vertical lines mark lineouts at constant duration/detuning ratio, which are shown in the lower/left panels. As the pulse duration exceeds the quantum beat period, the peaks become spectrally resolvable, and the total overlap at the central frequency becomes half of that at vanishing pulse duration. The peaks appearing below $d \approx 0.9$ occur when the lower harmonic excites autoionizing Rydberg states between ${}^2P_{3/2}$ and ${}^2P_{1/2}$ thresholds.

3.3 Maximum coherence achievable. Degree of coherence.

As seen in figure 4, given that the resonance condition $d = 1$ is fulfilled, the coherence between the ionization channels seem to increase as long as the pulse is of appreciable amplitude. What is the maximum coherence achievable using this scheme? The theoretical maximum coherence $|\rho_{mn}| = |c_m c_n^*|$, is bounded by the Cauchy–Schwartz inequality:

$$|\rho_{mn}|^2 \leq \rho_{mm}^2 \rho_{nn}^2, \quad (12)$$

where ρ_{ii} is the probability of finding the system in state $|i\rangle$, which obviously cannot exceed unity. From (12), it is natural to introduce the *degree of coherence*:

$$\tilde{\rho}_{mn} \equiv \frac{|\rho_{mn}|}{\sqrt{\rho_{mm}\rho_{nn}}}, \quad (13)$$

which normalizes the coherence between two ions to their respective populations. This quantity is useful since, even though the populations in two states are minuscule (as is the case in figure 4) and thereby also the absolute coherence, they may be fully coherent *with respect to each other*. If this is the case, the degree of coherence will be unity.

Figure 5 shows the degree of coherence, as a function of XUV pulse duration and detuning ratio. For short pulse durations, this quantity is larger than $\frac{1}{2}$ (left panel of figure 5). In this regime, the interaction with the XUV pulse occurs within one quantum beat period (3.2 fs), and the four pathways into the continuum (indicated in figure 3) have a partial spectral overlap. For larger pulse durations, two of the pathways become distinguishable, and do not contribute to the coherence between the ionic substates. The two remaining pathways, namely via $\Omega_{<}$ leaving the ion in ${}^2P_{3/2}^o$, and via $\Omega_{>}$ leaving the ion in ${}^2P_{1/2}^o$, cannot be distinguished when measuring the photo-electron. Provided the resonance condition $d = 1$ is met, the maximum degree of coherence is $\frac{1}{2}$. Complete decoherence always occurs in the long-pulse limit if $d \neq 1$ since the quantum pathways are distinguishable. As we will see below, the maximum degree of coherence can be increased by adding more colours to the ionizing field.

4 THE MULTI-COLOUR CASE — IONIZATION BY AN ATTOSECOND PULSE TRAIN

We consider now the effect of ionization with an attosecond pulse train, by including additional harmonic components. To focus on this aspect of the problem, we use a simplified model, where the dipole matrix elements for ionization are replaced with Heaviside functions (this is an approximation of a flat continuum, i.e. no resonances present):

$$z(\varepsilon) = \theta(\varepsilon), \quad (14)$$

where ε , as before, is the energy of the continuum electron. We still use the *Ansatz* (4), albeit with a compact notation only considering different channels n :

$$|\Psi(t)\rangle = c_0(t)|\Psi_0\rangle + \sum_n \int d\varepsilon c_n(t; \varepsilon)|n\varepsilon\rangle. \quad (15)$$

Inserting this in the Schrödinger equation and applying first-order time-dependent perturbation theory (i.e. the ground state is unaffected by the weak-field ionization; $c_0(t) = 1$), the solution reads

$$c_n(t) = -i\theta(\varepsilon) \int_{-\infty}^t dt' \mathcal{E}(t') \exp(iE_n t'). \quad (16)$$

Evaluating at the time of measurement ($t = +\infty$), we see that the coefficient becomes the Fourier transform of the driving field, evaluated at $-E_n - \varepsilon$. From this, we get the coherence between two channels (m, n) as

$$\rho_{mn} = - \int d\varepsilon \theta(\varepsilon) \hat{\mathcal{E}}^*(E_m + \varepsilon) \hat{\mathcal{E}}(-E_n - \varepsilon), \quad (17)$$

where $\hat{\mathcal{E}}(\omega)$ designates the Fourier transform of $\mathcal{E}(t)$. This expression shows that the coherence primarily arises from a correlation of the field with itself shifted by the energy difference $\Delta E \equiv E_m - E_n$.

In the long-pulse limit, the spectral components of $\hat{\mathcal{E}}(\omega)$ will become very narrow. If the ionizing field is an attosecond pulse train, consisting of the $n_q = q_2 - q_1 + 1$ successive harmonic orders $q \in \{q_1..q_2\}$, the shift has to be precisely an integer amount of photons ($\Delta E = N\omega_0$) for the integrand of (17) to be non-zero. Assuming $q_1\omega_0, q_2\omega_0 > E_m, E_n$, i.e. all constituent harmonic orders reach above both ionization thresholds, we have in total $2n_q$ pathways into the continuum. In the case of an integer photon shift, $2(n_q - N)$ of these pathways will overlap, which means

$$\tilde{\rho}_{mn} = \frac{n_q - N}{n_q}. \quad (18)$$

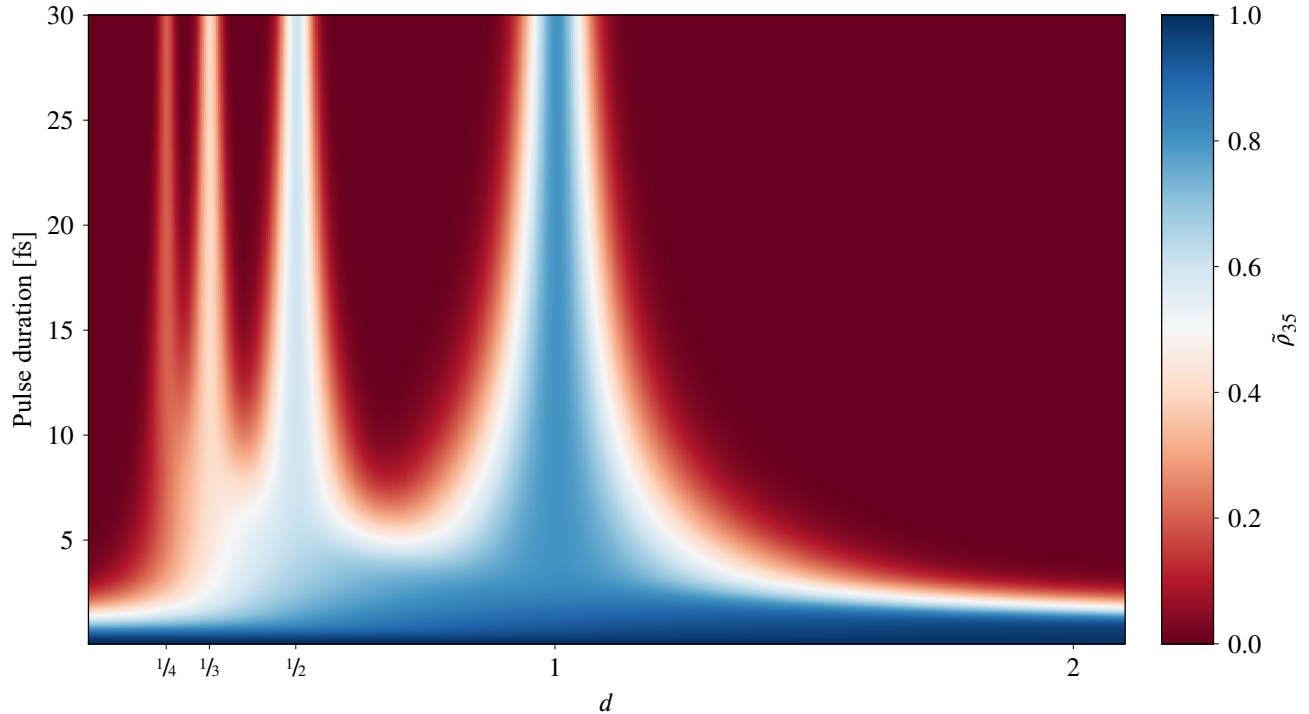


Figure 6: The effect of using five harmonics: At $d = 1$, 4 harmonics out of 5 will yield photo-electron peaks that overlap with those shifted by the spin-orbit splitting. The peaks appearing at $d = 1/4, 1/3, 1/2$ correspond to 1, 2, and 3 harmonics resulting in overlapping photo-electron peaks, respectively. In the time domain, this corresponds to ionizing pulses arriving at every $r = 4, 3, 2$ quantum beat periods.

From (18), we see that by adding more and more colours, we can increase the degree of coherence towards unity. This is illustrated in figure 6 for the case of five harmonics; the maximum degree of coherence is indeed $4/5$, which occurs at $d = 1$.

Figure 6 also serves the purpose of illustrating the generalization of the quantum beat condition (11); e.g. the case $r = 2$ corresponds in the time domain to ionizing pulses arriving every other quantum beat period. Such a field can be realized through red-blue HHG (resulting in odd *and* even harmonic orders) from a fundamental frequency $\Delta E_{s-o}/2$ (for Xe with $\Delta E_{s-o} \approx 1.3$ eV, a fundamental driving wavelength $\lambda \approx 1.9$ μm would thus be necessary). From this we see that in the spectral domain, the generalized quantum beat condition (11) is simply $d = 1/r$, $r \in \mathbb{Z}$.

Finally, we have also checked that in the long-pulse limit, the case of $d = 1/2$, using only odd-order harmonics is no different from the case of $d = 1$, using even- and odd-order harmonics. Thus the change of parity (phase difference) of consecutive pulses in the attosecond pulse train has no impact on the coherence, and we conclude that the degree of coherence is essentially dictated by the amount of indiscernible pathways.

5 CONCLUSION

In summary, we have shown that it is possible to induce coherence between two ionic substates using pulses of duration longer than the quantum beat time of their superposition. This is possible, provided a resonance condition is fulfilled, namely that the driving field has at least two frequency components spaced by precisely the energy difference of the levels of interest. This result shows

that when the electron wave packets arising from different pathways have the same kinetic energy, we cannot know which way the ionization occurred. This situation is reminiscent of a Young’s double slit experiment [see for instance Arndt et al. (2005)], with the two harmonic orders playing the roles of the two slits. It has to be noted, however, that no interference can be detected in the photo-electron signal, unless the ions are brought to the same final state via some mechanism [e.g. Goulielmakis et al. (2010) did this by further exciting from the fine structure superposition using an XUV pulse]. Otherwise, it would be possible to detect the ions and the photo-electrons in coincidence mode and establishing the ionization pathway.

6 ACKNOWLEDGMENTS

We acknowledge the help of Oleg Zatsarinny, and would like to thank Andreas Buchleitner, Andreas Wacker, Kevin Dunseath, Mikhail Ivanov, Tobias Brünner, and Tomas Brage for fruitful discussions. This work was supported by the Swedish Foundation for Strategic Research, the Swedish Research Council, the Knut and Alice Wallenberg Foundation, the European Research Council (PALP), and by funding from the NSF under grant PHY-1307083.

REFERENCES

- Alvermann, A., Fehske, H., and Littlewood, P. B. (2012). ‘Numerical time propagation of quantum systems in radiation fields’. *New Journal of Physics* **14**.10, p. 105008. DOI: [10.1088/1367-2630/14/10/105008](https://doi.org/10.1088/1367-2630/14/10/105008).
- Arndt, M., Hornberger, K., and Zeilinger, A. (2005). ‘Probing the limits of the quantum world’. *Physics World* **18**.3, pp. 35–40. DOI: [10.1088/2058-7058/18/3/28](https://doi.org/10.1088/2058-7058/18/3/28).
- Cowan, R. (1981). *The theory of atomic structure and spectra*. Berkeley: University of California Press. ISBN: [0520038215](https://doi.org/10.1016/j.cpc.2007.01.006).
- Froese Fischer, C., Tachiev, G., Gaigalas, G., and Godefroid, M. R. (2007). ‘An MCHF atomic-structure package for large-scale calculations’. *Computer Physics Communications* **176**.8, pp. 559–579. DOI: [10.1016/j.cpc.2007.01.006](https://doi.org/10.1016/j.cpc.2007.01.006).
- Goulielmakis, E., Loh, Z.-H., Wirth, A., Santra, R., Rohringer, N., Yakovlev, V. S., Zherebtsov, S., Pfeifer, T., Azzeer, A. M., Kling, M. F., Leone, S. R., and Krausz, F. (2010). ‘Real-time observation of valence electron motion’. *Nature* **466**.7307, pp. 739–743. DOI: [10.1038/nature09212](https://doi.org/10.1038/nature09212).
- Klünder, K., Johnsson, P., Swoboda, M., L’Huillier, A., Sansone, G., Nisoli, M., Vrakking, M. J., Schafer, K. J., and Mauritsson, J. (2013). ‘Reconstruction of attosecond electron wave packets using quantum state holography’. *Physical Review A* **88**.3, p. 033404. DOI: [10.1103/PhysRevA.88.033404](https://doi.org/10.1103/PhysRevA.88.033404).
- Kurka, M., Rudenko, A., Foucar, L., Kühnel, K., Jiang, Y., Ergler, T., Havermeier, T., Smolarski, M., Schössler, S., Cole, K., et al. (2009). ‘Two-photon double ionization of Ne by free-electron laser radiation: a kinematically complete experiment’. *Journal of Physics B: Atomic, Molecular and Optical Physics* **42**.14, p. 141002.
- Landau, L. D. and Lifshitz, E. M. (1977). *Quantum mechanics : non-relativistic theory*. 3rd. Vol. 3. Course of Theoretical Physics. Oxford New York: Pergamon Press. ISBN: [978-0-08-020940-1](https://doi.org/10.1002/cpa.3160070404).
- Magnus, W. (1954). ‘On the exponential solution of differential equations for a linear operator’. *Communications on Pure and Applied Mathematics* **7**.4, pp. 649–673. DOI: [10.1002/cpa.3160070404](https://doi.org/10.1002/cpa.3160070404).
- Mauritsson, J., Remetter, T., Swoboda, M., Klünder, K., L’Huillier, A., Schafer, K. J., Ghafur, O., Kelkensberg, F., Siu, W., Johnsson, P., Vrakking, M. J. J., Znakovskaya, I., Uphues, T., Zherebtsov, S., Kling, M. F., Lépine, F., Benedetti, E., Ferrari, F., Sansone, G., and Nisoli, M. (2010). ‘Attosecond Electron Spectroscopy Using a Novel Interferometric Pump-Probe Technique’. *Physical Review Letters* **105** (5), p. 053001. DOI: [10.1103/PhysRevLett.105.053001](https://doi.org/10.1103/PhysRevLett.105.053001).

- Nikolopoulos, L. A. A. (2013). ‘Time-Dependent Theory of Angular Correlations in Sequential Double Ionization’. *Physical Review Letters* **111**.9. DOI: [10.1103/physrevlett.111.093001](https://doi.org/10.1103/physrevlett.111.093001).
- Pabst, S., Greenman, L., Ho, P. J., Mazziotti, D. A., and Santra, R. (2011). ‘Decoherence in Attosecond Photoionization’. *Physical Review Letters* **106**.5. DOI: [10.1103/physrevlett.106.053003](https://doi.org/10.1103/physrevlett.106.053003).
- Pabst, S., Lein, M., and Wörner, H. J. (2016). ‘Preparing attosecond coherences by strong-field ionization’. *Physical Review A* **93**.2. DOI: [10.1103/physreva.93.023412](https://doi.org/10.1103/physreva.93.023412).
- Saad, Y. (1992). ‘Analysis of some Krylov subspace approximations’. *SIAM Journal on Numerical Analysis*.
- Salour, M. and Cohen-Tannoudji, C. (1977). ‘Observation of Ramsey’s interference fringes in the profile of Doppler-free two-photon resonances’. *Physical Review Letters* **38**.14, p. 757. DOI: [10.1103/PhysRevLett.38.757](https://doi.org/10.1103/PhysRevLett.38.757).
- Teets, R., Eckstein, J., and Hänsch, T. (1977). ‘Coherent two-photon excitation by multiple light pulses’. *Physical Review Letters* **38**.14, p. 760.
- Tzallas, P., Skantzakis, E., Nikolopoulos, L. A. A., Tsakiris, G. D., and Charalambidis, D. (2011). ‘Extreme-ultraviolet pump-probe studies of one-femtosecond-scale electron dynamics’. *Nature Physics* **7**.10, pp. 781–784. DOI: [10.1038/nphys2033](https://doi.org/10.1038/nphys2033).
- Zatsarinny, O. (2006). ‘BSR: B-spline atomic R-matrix codes’. *Computer Physics Communications* **174**.4, pp. 273–356. DOI: [10.1016/j.cpc.2005.10.006](https://doi.org/10.1016/j.cpc.2005.10.006).
- Zatsarinny, O. and Froese Fischer, C. (2009). ‘Atomic structure calculations using MCHF and BSR’. *Computer Physics Communications* **180**.11, pp. 2041–2065. DOI: [10.1016/j.cpc.2009.06.007](https://doi.org/10.1016/j.cpc.2009.06.007).